



Density functional theory studies on the structures and electronic communication of *meso*-ferrocenylporphyrins: Long range orbital coupling *via* porphyrin core

Lijuan Zhang, Dongdong Qi, Yuexing Zhang, Yongzhong Bian*, Jianzhuang Jiang*

Department of Chemistry, University of Science and Technology Beijing, Beijing 100083, China

ARTICLE INFO

Article history:

Received 14 September 2010

Received in revised form 5 December 2010

Accepted 7 December 2010

Available online 17 December 2010

Keywords:

Density functional theory

Meso-attached ferrocenylporphyrins

Molecular orbital

Long range electronic coupling

Electronic absorption spectra

ABSTRACT

The molecular and electronic structures together with the electronic absorption spectra of a series of metal free *meso*-ferrocenylporphyrins, namely 5-ferrocenylporphyrin (**1**), 5,10-diferrocenylporphyrin (**2**), 5,15-diferrocenylporphyrin (**3**), 5,10,15-triferrocenylporphyrin (**4**), and 5,10,15,20-tetraferrocenylporphyrin (**5**) have been studied with the density functional theory (DFT) and time-dependent density functional theory (TD-DFT) methods. For the purpose of comparative studies, metal free porphyrin without any ferrocenyl group (**0**) and isolated ferrocene (**6**) were also calculated. The effects of the number and position of *meso*-attached ferrocenyl substituents on their molecular and electronic structures, atomic charges, molecular orbitals, and electronic absorption spectra of **1–5** were systematically investigated. The orbital coupling is investigated in detail, explaining well the long range coupling of ferrocenyl substituents connected *via* porphyrin core and the systematic change in the electronic absorption spectra of porphyrin compounds.

© 2010 Elsevier Inc. All rights reserved.

1. Introduction

Discrete molecular systems containing multiple photo- and redox-active centers with long range electronic coupling have received considerable attention in recent years due to their potential applications in molecular electronic devices [1–4]. Ferrocene has been widely used in the construction of such multi-component systems for the purpose of detecting and investigating the metal–metal coupling due to its unique structural and well-defined redox behavior [5–7]. Porphyrins [8–12] and their most important artificial analogues, phthalocyanines [13], are ideal frameworks linking the redox-active metallocenyl units including ferrocenyl substituents due to their special molecular structure, electrochemical, and photophysical properties. For the purpose of constructing novel supermolecular structures with novel multi-functional properties, combination of these two functional subunits, i.e. porphyrin core and ferrocenyl unit(s), has attracted increasing research interest since last century [14,15].

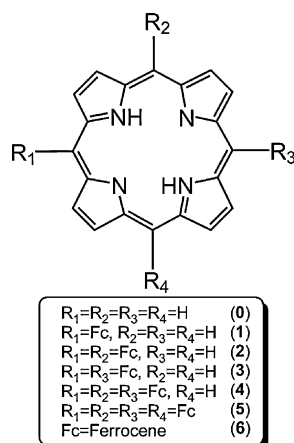
Experimental investigations have revealed that effective long range electronic coupling between ferrocenyl units linked *via* porphyrin framework was retarded to some degree probably by the not close enough distance and unsuitable relative orientation due to

the unlimited free rotation of the ferrocenyl units [12,15,16]. This, however, has not yet been confirmed from the point of theoretical investigation because of the lack of theoretical calculations in this regard. On the other hand, density functional theory (DFT) and time dependant density functional theory (TD-DFT) methods have proved suitable for the calculation of the energy-minimized structures, electronic distribution, molecular orbitals, electron transfer, and electronic absorption spectra of a series of porphyrin and phthalocyanine derivatives [17–23] as well as ferrocene derivatives [24–29]. As a consequence, towards understanding the long range electronic coupling between ferrocenyl groups connected *via* porphyrin framework, theoretical studies over multi-component compounds composed of porphyrin and ferrocenyl units appear interesting. It is worth noting that during review process of the present paper, Nemykin et al. synthesized and characterized a series of free-based *meso*-poly(ferrocenyl)-containing porphyrin [30] and studied the electron absorption spectra of these series compounds with DFT method [31], which provide a good chance for comparing our calculation result with the experimental and previous computational data despite that detailed studies on the electronic structures and orbital coupling of the series of compounds were not included.

In the present paper, density functional theory (DFT) and time-dependent density functional theory (TD-DFT) calculations were carried out on the basis of the molecular and electronic structures, interaction between the porphyrin core and ferrocenyl substituent(s), long range electronic interaction

* Corresponding authors. Tel.: +86 10 6233 4509; fax: +86 10 6233 2462.

E-mail addresses: yzbian@ustb.edu.cn (Y. Bian), jianzhuang@ustb.edu.cn (J. Jiang).



Scheme 1. Schematic molecular structures of **0–6**.

between ferrocenyl groups, and electronic absorption spectra of a series of metal free *meso*-ferrocenylporphyrins, namely 5-ferrocenylporphyrin (**1**), 5,10-diferrocenylporphyrin (**2**), 5,15-diferrocenylporphyrin (**3**), 5,10,15-triferrocenylporphyrin (**4**), and 5,10,15,20-tetraferrocenylporphyrin (**5**), **Scheme 1**. For the purpose of comparative studies, metal free porphyrin without any ferrocenyl group (**0**) and isolated ferrocene (**6**) molecule were also calculated.

2. Computational details

Density functional theory (DFT) method of hybrid B3LYP [32,33] functional with Becke exchange and Lee–Yang–Parr correlation was used to calculate the molecular structures of the series of *meso*-ferrocenyl porphyrins. The LACVP(d) basis set [34,35], which is a combination of the 6-31G(d) basis set for C/H/N with the LanL2DZ effective core basis set for Fe, was chosen. The B3LYP functional method with LACVP(d) basis set is proved suitable for geometry optimizations of porphyrins [17–20] and ferrocenyl-containing systems [28,29]. The Berny algorithm using redundant internal coordinates [36] was employed in energy minimization and the default cutoffs were used throughout. No imaginary vibration is predicated in the following frequency calculations of the IR vibration spectroscopy, indicating that the energy-minimized structures for all of the complexes are true energy minima. Natural bond orbital (NBO) analysis [37] was carried out with NBO 3.1 [38] in Gaussian 03 program [39] on the basis of the minimized structures.

The electronic structures and electronic absorption spectra were calculated using DFT method of Beck's exchange functional [32]

and Perdew–Wang correlation functional (BPW91) [40]. The 6-311+G(d) basis set for Fe atom and 6-311G(d) basis set for all other atoms was employed. All calculations were carried out using the Gaussian 03 program [39] on an IBM P690 system housed at Shandong Province High Performance Computing Center.

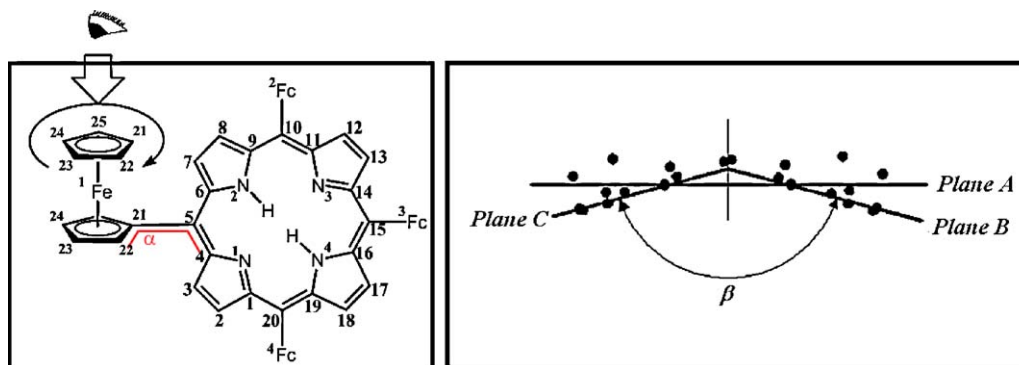
The total electron density difference between ground and excited states ($\sum f_{m \rightarrow n}$) is calculated by the molecular orbital electron density difference with formula $f_{m \rightarrow n} = (c_{m \rightarrow n}^2 / \sum c_{m \rightarrow n}^2)(\rho_n - \rho_m)$, where ρ_n and ρ_m are the electron density of the two molecular orbitals relative to the electron transition model of $MO(m) \rightarrow MO(n)$, $c_{m \rightarrow n}$ is the orthogonal coefficient in the TD-DFT equation, and then $(c_{m \rightarrow n}^2 / \sum c_{m \rightarrow n}^2)$ can be considered as the contribution of this electron transition model to this absorption peak. The electron density difference between ground and excited states is the linear combination of various electron transition models. Also for the reason of time efficiency, only the electron transition models with the configuration larger than 5.0% are taken into account. The electron density difference map is plotted using the isovalue of $4.0 \times 10^{-4} \text{ e au}^3$.

3. Results and discussion

3.1. Molecular structures

Table S1 (Supporting Information) compares the calculated structural parameters of **5** with those revealed by single crystal X-ray diffraction analysis [30]. As can be found, the largest difference of atom distance and bond angle for ferrocenyl substituents between the calculated and experimental data is only 0.06 Å for Fe–C22 and 0.7° for C28–C29–C30 in **5**, respectively, indicating the reliable simulated molecular structures at the level of B3LYP/LACVP(d).

In the metal free porphyrin without any ferrocenyl unit **0**, the central porphyrin core possesses a complete planar structure. However, as can be found in **Table 1**, the original planar porphyrin core becomes distorted due to the introduction of ferrocenyl substituent(s) onto the *meso*-positions of porphyrin ring. As shown in **Scheme 2**, the torsion angle β defined as the dihedral angle between plane B (defined by N1, N4, and C20) and plane C (defined by N3, N2, and C10) is employed to describe the nonplanarity for the porphyrin core of *meso*-ferrocenylporphyrins **1–5**. Along with the increase in the *meso*-attached ferrocenyl groups from one, two, three, to four for **1**, **2** (**3**), **4**, and **5**, the torsion angle β increases from 6.3, 13.5 (11.7), 22.4, to 30.6° , revealing the increased distortion of the porphyrin core in the same order due to the increased steric hindrance, **Table 1**. Nevertheless, an excellent linear relationship exists between the torsion angle (β) and the number of *meso*-attached ferrocenyl substituents, **Fig. S1 (Supporting Information)**.



Scheme 2. Atom labeling of **5** as a typical representative. Inclination angle C22–C21–C5–C4 (α) shows the torsion angle between ferrocenyl units and porphyrin core. Plane A is the average plane of the four inner nitrogen atoms. Plane B is defined by N1, N4 and C20. Plane C is defined by N3, N2, and C10. Torsion angle β is the dihedral angle between plane B and plane C.

Table 1Main structural parameters for the calculated structures of **1–6**.

Parameters	6	1	2		3	4			5	
	Fc	Fc1	Fc1	Fc2	Fc1/Fc2	Fc1	Fc2	Fc3	Fc1/Fc3	Fc2/Fc4
Fe1–C21	2.08	2.13	2.13	2.13	2.13	2.13	2.13	2.12	2.12	2.12
Fe1–C22	2.08	2.07	2.07	2.10	2.07	2.07	2.07	2.10	2.07	2.09
Fe1–C23	2.08	2.07	2.07	2.08	2.07	2.07	2.06	2.08	2.07	2.08
Fe1–C24	2.08	2.08	2.08	2.07	2.08	2.08	2.08	2.07	2.08	2.07
Fe1–C25	2.08	2.10	2.10	2.07	2.10	2.10	2.10	2.07	2.10	2.07
Fe1–C26	2.08	2.09	2.09	2.09	2.09	2.09	2.09	2.09	2.08	2.08
Fe1–C27	2.08	2.08	2.08	2.09	2.08	2.07	2.08	2.09	2.08	2.09
Fe1–C28	2.08	2.08	2.08	2.08	2.08	2.08	2.08	2.08	2.08	2.08
Fe1–C29	2.08	2.08	2.08	2.08	2.08	2.08	2.08	2.08	2.08	2.08
Fe1–C30	2.08	2.09	2.09	2.08	2.09	2.09	2.09	2.08	2.09	2.08
C21–C22	1.43	1.44	1.44	1.44	1.44	1.44	1.44	1.44	1.44	1.44
C22–C23	1.43	1.43	1.43	1.43	1.43	1.43	1.43	1.43	1.43	1.43
C23–C24	1.43	1.43	1.43	1.43	1.43	1.43	1.43	1.43	1.43	1.43
C24–C25	1.43	1.43	1.43	1.43	1.43	1.43	1.43	1.43	1.43	1.43
C25–C21	1.43	1.44	1.44	1.44	1.44	1.44	1.44	1.44	1.44	1.44
C26–C27	1.43	1.43	1.43	1.43	1.43	1.43	1.43	1.43	1.43	1.43
C27–C28	1.43	1.43	1.43	1.43	1.43	1.43	1.43	1.43	1.43	1.43
C28–C29	1.43	1.43	1.43	1.43	1.43	1.43	1.43	1.43	1.43	1.43
C29–C30	1.43	1.43	1.43	1.43	1.43	1.43	1.43	1.43	1.43	1.43
C30–C26	1.43	1.43	1.43	1.43	1.43	1.43	1.43	1.43	1.43	1.43
Fe–Q1 ^a	1.69	1.70	1.70	1.70	1.70	1.70	1.70	1.70	1.69	1.69
Fe–Q2 ^a	1.69	1.69	1.69	1.69	1.69	1.69	1.69	1.69	1.69	1.69
Q1–Fe–Q2	180.0	176.7	176.7	176.7	177.0	176.9	176.6	177.1	177.4	177.3
C25–C21–C22	108.0	106.4	106.3	106.3	106.4	106.4	106.3	106.4	106.4	106.3
C21–C22–C23	108.0	109.0	109.0	108.9	109.0	109.0	109.0	108.8	108.8	109.0
C22–C23–C24	108.0	107.8	107.8	108.0	107.8	107.8	107.7	108.0	108.1	107.8
C23–C24–C25	108.0	108.0	108.0	107.7	108.0	108.0	108.0	107.8	107.8	108.1
C24–C25–C21	108.0	108.9	108.9	109.0	108.8	108.9	108.9	109.0	109.0	108.9
C30–C26–C27	108.0	108.0	108.0	108.0	108.0	108.0	108.0	108.0	108.0	108.0
C26–C27–C28	108.0	108.0	108.0	108.1	108.0	108.0	108.0	108.1	108.1	108.0
C27–C28–C29	108.0	108.0	108.1	107.9	108.0	108.0	108.0	107.9	107.9	108.0
C28–C29–C30	108.0	107.9	107.9	108.0	107.9	107.9	107.9	108.0	108.0	107.9
C29–C30–C26	108.0	108.3	108.1	108.0	108.0	108.1	108.1	108.0	108.0	108.1
α^b	/	42.9	41.4	44.7	42.4	46.1	45.2	43.9	42.0	42.0
β^b	/	6.3	13.5	11.7	22.4	30.6				

^a Q1 and Q2 represent the center of the bottom and above cyclopentadienyl moieties of *meso*-attached ferrocenyl substituents.^b The definition of the torsion angles α and β is available in Scheme 1.

As expected, the *meso*-attached ferrocenyl units in **1–5** also become slightly distorted from the original structure of isolated ferrocene (**6**). As tabulated in Table 1, the ferrocenyl units attached at the *meso*-positions of porphyrin ring in **1–5** lose the relatively higher symmetry of D_{5d} for the isolated ferrocene molecule due to the steric hindrance of the porphyrin core. This is clearly revealed by the Q1–Fe–Q2 angle (in which Q1 and Q2 denote the center of the bottom and above cyclopentadienyl moieties of ferrocenyl unit, respectively) in the range of 2.6–3.4° for the *meso*-attached ferrocenyl substituents in the metal free porphyrin compounds **1–5**.

It is well known that the electronic communication between the ferrocenyl substituents and porphyrin core is influenced by their relative positions [41–43]. For this purpose, the torsion angle between ferrocenyl units and porphyrin core is defined by the inclination angle like C22–C21–C5–C4 (α) in **1–5**, Scheme 2. The α value for the whole series of metal free porphyrin compounds was revealed to locate in the range of 41.4–46.1° according to our calculations, which is smaller than that between the phenyl group and porphyrin core in 5,10,15,20-tetra(phenyl)porphyrin, H₂TPP, 60.6–62.2°, as revealed by the single crystal X-ray diffraction analysis [42], indicating the more effective electronic communication between *meso*-attached substituents and porphyrin core in **1–5** than in H₂TPP.

3.2. Atomic charge distribution

Full natural bond orbital (NBO) analyses are carried out to determine the influence of the number and position of the *meso*-attached ferrocenyl substituents on the charge distribution. As organized in

Table 2 and S2 (Supporting Information), the charge of Fe atom in the range between +0.22 e and +0.24 e in **1–5** is very similar to that in isolated ferrocene compound **6**, +0.23 e. The charges of the inner N with H atom, inner N without H atom, and inner H of the porphyrin core for **1–5** are calculated to be about –0.58 e, –0.53 e, and +0.47 e, respectively, which remain almost unchanged in comparison with those of metal free porphyrin without any *meso*-attached ferrocenyl substituent **0**, indicating the little influence of the *meso*-attached ferrocenyl substituents to the charge distribution of the molecular center in terms of atom charge distribution. In contrast, the negative charge of the *meso*-carbons decreases from –0.24 e for the metal free porphyrin (**0**) to –0.05 e for *meso*-attached ferrocenyl porphyrins **1–5**, revealing the decreased charge distribution of porphyrin skeleton associated with the ferrocenyl substituents. In a similar manner, the negative charge of the carbon atom in ferrocenyl groups which is directly connected to the *meso*-carbon of porphyrin core also decreases from –0.28 e for isolated ferrocene **6** to –0.10 e for ferrocenyl units attached to porphyrin in **1–5**, indicating the charge redistribution around the two carbon

Table 2Total atomic charges (in e) for **0–5**. *Meso*-1, *meso*-2, *meso*-3, and *meso*-4 denote the *meso*-attached ferrocenyl substituents or hydrogen atoms on four *meso*-positions.

Parameters	0	1	2	3	4	5
<i>meso</i> -1	0.24	0.01	0.01	0.24	0.01	0.01
<i>meso</i> -2	0.24	0.24	0.01	0.01	0.01	0.02
<i>meso</i> -3	0.24	0.24	0.24	0.24	0.01	0.01
<i>meso</i> -4	0.24	0.24	0.24	0.01	0.24	0.02
Porphyrin core	–0.97	–0.74	–0.50	–0.50	–0.27	–0.06

atoms directly connecting the ferrocenyl and porphyrin units in these multi-component porphyrin compounds. In addition, the total charge of ferrocenyl substituents changes from a negative value of -0.26 e in the isolated ferrocene (**6**) to a small positive value of $+0.01\text{ e}$ in *meso*-ferrocenylporphyrins (**1–5**). In the case of porphyrin core, the total charge decreases from -0.97 e for **0**, -0.74 e for **1**, $-0.05(-0.05)\text{ e}$ for **2(3)**, -0.27 e for **4**, to -0.06 e for **5**, respectively. A good-quality linear correlation between the total charge of porphyrin core and the number of ferrocenyl units is observed, Fig. S1 (Supporting Information), indicating the more the number of ferrocenyl substituents is, the lower the negative charge on the porphyrin core is. The very small value of charge distribution on ferrocenyl substituent(s) and porphyrin core reveals the similar electronegativity for porphyrin core and ferrocenyl substituent.

3.3. Molecular orbitals

In order to gain an insight into the electron communications between the porphyrin core and ferrocenyl unit(s), the orbital interaction between the porphyrin core and ferrocenyl unit in metal free porphyrin **1**, as a typical representative of the series of *meso*-ferrocenylporphyrins **1–5**, is discussed in terms of the molecular orbital distribution and energy levels of **0**, **1**, and **6**, Fig. 1 and S2 (Supporting Information). The frontier orbitals of **1** are formed from the corresponding orbitals of **0** and **6**. When ferrocene (**6**) is connected with porphyrin **0** to form *meso*-ferrocenylporphyrin **1**, the HOMO(81) and HOMO–1(80) of **0** become the HOMO–3(125) and HOMO–4(124) of **1**, with slight contribution from the *d* orbitals of **6**. In comparison with HOMO(81) and HOMO–1(80) of **0**, the energy of HOMO–3(125) and HOMO–4(124) of **1** increases slightly by 0.07 and 0.06 eV, respectively, due to the slight coupling between HOMO(81)/HOMO–1(80) of **1** and the *d* orbitals of **6**. The HOMO(48), HOMO(47), and HOMO–2(46) of **6**, which belong to the iron-centered $d_{x^2-y^2}$, d_{xy} , and d_{z^2} orbitals (Fig. S2 in Supporting Information), become the HOMO(128), HOMO–1(127), and HOMO–2(126) of **1**, respectively, with a small contribution of the HOMO(81) of **0**. In other words, the HOMO(128), HOMO–1(127), and HOMO–2(126) of **1** are mainly localized on the ferrocenyl substituents while the HOMO–3(125) and HOMO–4(124) orbitals of **1** are almost independently composed from the HOMO and HOMO–1 orbitals of porphyrin core, indicating the slight electronic communication between the *meso*-attached ferrocenyl unit(s) and porphyrin core. Because of the much lower energy level (around 1.5 eV lower) of the LUMOs(82,83) of **0** in comparison with the LUMOs(49,50) of **6**, the LUMO(129) and LUMO+1(130) of **1** are

almost separately formed from the LUMOs(82,83) of **0** with little contribution from the LUMO(49) of **6**. In addition, the introduction of *meso*-attached ferrocenyl substituent destroys the approximate degeneracy for LUMOs(82,83) of **0**, leading to a separation of 0.08 eV between LUMO(129) and LUMO+1(130) in **1**.

The molecular orbitals of **2–5** can be understood in a similar way as those of **1**. That is, the orbitals from HOMO to HOMO–5 for **2/3**, from HOMO to HOMO–8 for **4**, and from HOMO to HOMO–11 for **5**, are basically ferrocenyl-centered orbitals with little contribution from the porphyrin core, while the following occupied orbitals and the LUMO/LUMO+1 orbitals of **2–5** are porphyrin core-centered orbitals formed from the HOMO/HOMO–1 orbitals (81,80) and LUMOs(83,82) of **0**. These results imply the similar and slight molecular orbital coupling between the frontier orbitals of porphyrin core and ferrocenyl units for the series of compounds **2–5** in comparison with **1**.

Despite the low orbital coupling degree of the porphyrin core and ferrocenyl units in **1–5**, the orbital energies of these compounds are significantly affected by the ferrocenyl units. As can be seen from Table S3 (Supporting Information), the energies of porphyrin core-centered occupied orbitals of **0–5** increase by about 0.07 eV per ferrocenyl unit along with the increase in the number of ferrocenyl substituents, indicating the slightly electron-donating nature of ferrocenyl units relative to porphyrin core. However, the energies of LUMOs keep almost unchanged along with the same order. As detailed below, the almost degenerated LUMO and LUMO+1 orbitals of **0** become nondegenerate after the introduction of *meso*-attached ferrocenyl unit(s), Fig. 2. As a result, the energy gap between the highest occupied porphyrin-centered orbital and the LUMO decreases from 1.95 for **0** to 1.87 for **1**, 1.86(1.81) for **2(3)**, 1.81 for **4**, and 1.77 eV for **5**, suggesting the red-shift of the porphyrin Q absorption band in their electronic absorption spectra of **0–5** along with the increase of ferrocenyl substituents. As detailed below, this is in line with their simulated electronic absorption spectroscopic results.

As mentioned above, the introduction of *meso*-ferrocenyl substituents onto the *meso*-positions of porphyrin ring induces energy splitting for the almost degenerated LUMO and LUMO+1 in porphyrin compound **0** as a result of the asymmetric substitution. In terms of $\Delta E_{(\text{LUMO}+1)-(\text{LUMO})}$ energy gap, the splitting degree of LUMO and LUMO+1 can be divided into three types: the slight splitting for **2** and **5**, the moderate splitting for **1** and **4**, and the large splitting for **3**. As shown in Fig. 2, the LUMO for **2** with two neighboring *meso*-attached ferrocenyl substituents are revealed to equally extend and equally distribute over its two *meso*-ferrocenyl substituents, this is also true for the LUMO+1 of this compound. Due to the symmetric orbital extension, the gap between LUMO and LUMO+1 is only 0.02 eV. As expected, both the LUMO and LUMO+1 for **5** with four (two pairs of neighboring) *meso*-attached

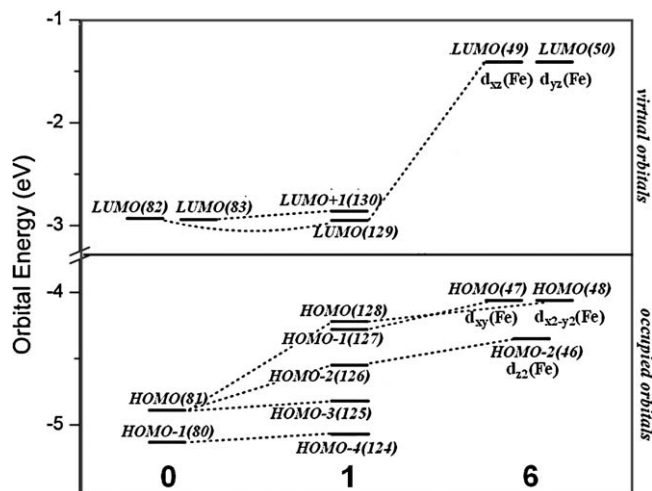


Fig. 1. The orbital energy diagrams of **0**, **1**, and **6**.

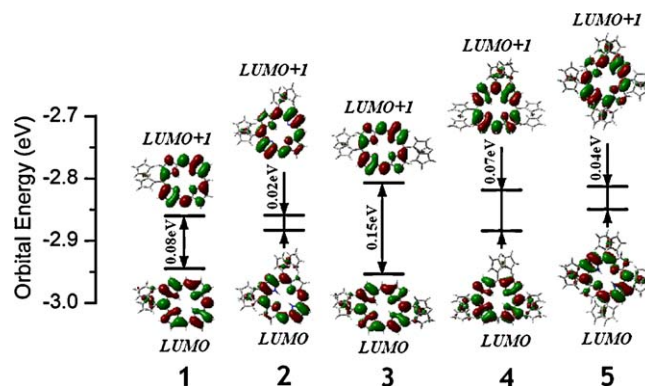


Fig. 2. The energy splitting degree of LUMO and LUMO+1.

ferrocenyl substituents extend and distribute over two of its four *meso*-ferrocenyl substituents in a symmetric manner, respectively, therefore also leading to a slight orbital splitting between LUMO and LUMO+1 with the gap of 0.04 eV. In contrast, the LUMO distribution for **1** with only one *meso*-attached ferrocenyl substituent extends to its sole *meso*-ferrocenyl unit, while the LUMO+1 distribution is almost irrespective with the *meso*-ferrocenyl substituent. Such an asymmetric orbital extension results in an increased splitting between LUMO and LUMO+1 with the gap of 0.08 eV. Due to the same reason, asymmetric orbital extension for **4** bringing three *meso*-attached ferrocenyl substituents with its LUMO distribution extending to two of its three *meso*-ferrocenyl substituents and LUMO+1 distribution only to the third *meso*-ferrocenyl substituent also leads to a moderate orbital splitting between LUMO and LUMO+1 with the gap of 0.07 eV. As for the metal free porphyrin compound **3** with two opposite *meso*-attached ferrocenyl substituents, its LUMO distribution extends to both two *meso*-ferrocenyl substituents but LUMO+1 distribution is irrespective with any *meso*-attached ferrocenyl substituent, leading to much lower distribution extension of LUMO+1 than LUMO. This in turn results in the largest LUMO and LUMO+1 splitting with the gap of 0.15 eV among the series of porphyrin compounds **1–5**. These results clearly reveal the effect of the position and number of *meso*-attached ferrocenyl substituents on the energies of LUMO and LUMO+1 of resulting porphyrins.

3.4. Long range metal–metal coupling

The long range metal–metal coupling of 5,15-diferrocenylporphyrin (**3**) is discussed below as a representative example for the multi *meso*-ferrocenyl attached porphyrins (**2–5**). The orbital coupling degree is defined using the energy splitting of the coupled orbitals [44]. As is shown in Fig. 3, the HOMO(175) and HOMO–1(174) of **3** are coupled by the HOMO(48)s of the two ferrocenyl substituents, leading to an energy splitting with a gap of 0.08 eV between the HOMO(175) and HOMO–1(174) of **3**. Similarly, the HOMO(47)s of **6** are coupled to form the HOMO–2(173) and HOMO–3(172) of **3** with a slight energy splitting of 0.01 eV.

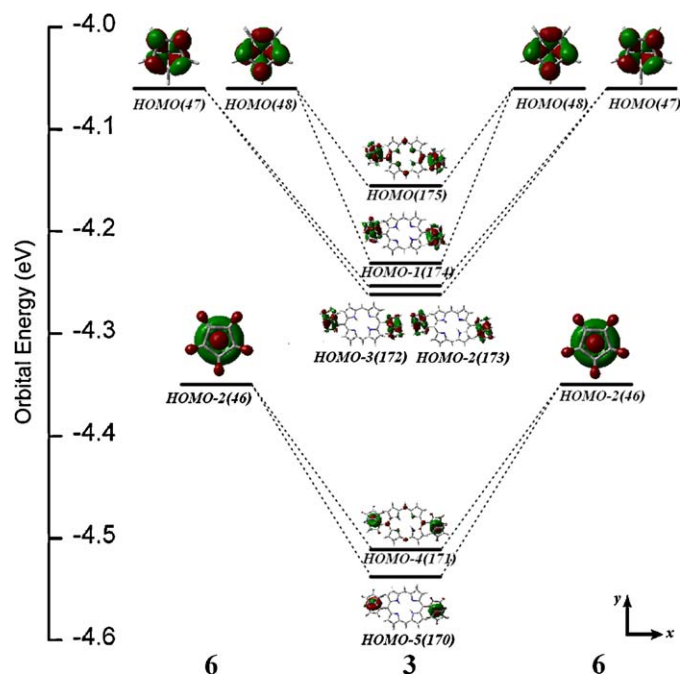


Fig. 3. The occupied frontier orbitals of **3** coupled by the corresponding orbitals of **6**.

The HOMO–4(171) and HOMO–5(170) of **1** are formed from the coupling of HOMO–2(46)s of **6** with an energy splitting of 0.03 eV. It must be pointed out that the energy of HOMO(175), HOMO–2(173), and HOMO–4(171) of **3** decreases by 0.10, 0.19, and 0.16 eV in comparison with the energy of HOMO(48), HOMO(47), and HOMO–2(46) of **6**, respectively. This type of energy decrease can be reasonably interpreted by the charge distribution of corresponding atoms or fragments, as discussed in Section 3.2. When the ferrocene is connected to the porphyrin, the electron density of ferrocene substituents is lower than the isolated ferrocene, leading to the energy decrease of ferrocenyl-centered HOMO(175), HOMO–2(173), and HOMO–4(171) of **3**. Due to the same number of ferrocenyl substituents contained, two neighboring *meso*-attached ferrocenyl porphyrin of **2** displays almost the same coupling with **3**.

Accordingly, the similar long range metal–metal coupling is also found in **4** and **5**. In the case of **4**, HOMO(222), HOMO–1(221), and HOMO–2(220) locate at the ferrocenyl substituents with iron-centered $d_{x^2-y^2}$ orbitals, due to the coupling of HOMO(48)s of the three ferrocenyl substituents, revealing a energy splitting of 0.10 eV. On the other hand, three HOMO(47)s of **6** are coupled to form HOMO–3(219), HOMO–4(218), and HOMO–5(216) of **4** (three iron-centered d_{xy} orbitals locating at the three *meso*-ferrocenyl substituents), with a energy splitting of 0.03 eV. The iron-centered d_{z^2} orbital HOMO–2(46)s of **6** form HOMO–6(215), HOMO–7(214), and HOMO–8(213) of **4** with a energy splitting of 0.05 eV. Similarly, in the case of **5**, coupling of HOMO(48), HOMO(47), and HOMO(46) of **6** forms three sets of orbitals (twelve orbitals) with the energy splitting of 0.17, 0.01, and 0.05 eV. The effective orbital overlap between frontier orbitals associated with the ferrocenyl substituents indicates a metal–metal interaction tendency. In general, the coupling degree increases along with the increasing number of ferrocenyl substituents (Fig. 4).

3.5. Electronic absorption spectra

The electronic absorption spectra of the series of metal free porphyrins **1–5** are simulated using TD-DFT method, Fig. 5 and Table S4 (Supporting Information). As can be found, the UV–vis spectra of **1–5** can be divided into three regions due to the different electron transition models. The absorptions in

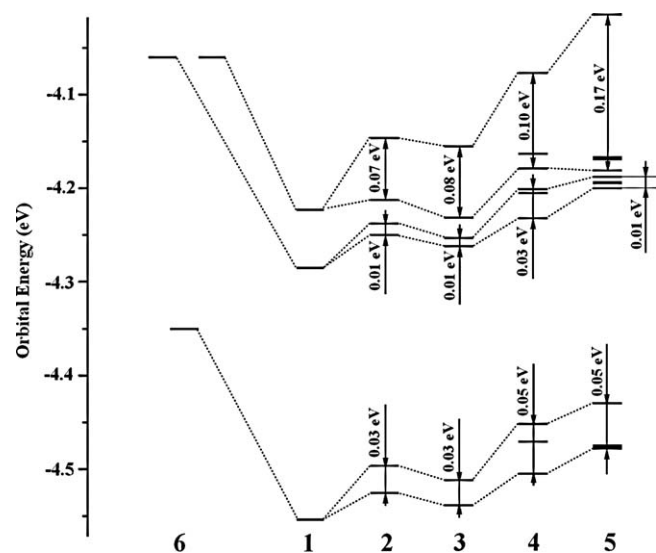


Fig. 4. The coupling degree of the ferrocenyl occupied orbitals: HOMO–2(46) to HOMO(48) for **6**, HOMO–2(126) to HOMO(128) for **1**, HOMO–5(170) to HOMO(175) for **2** (or **3**), HOMO–8(214) to HOMO(222) for **4**, HOMO–11(258) to HOMO(269) for **5**.

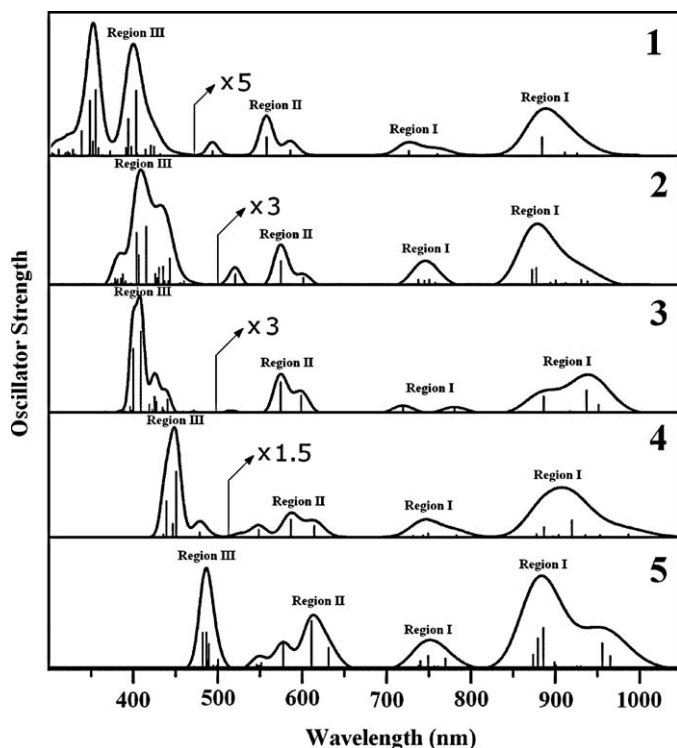


Fig. 5. Simulated electronic absorption spectra of 1–5.

Table 3
Electron density difference plots of electron transitions (isovalue: $4.0 \times 10^{-4} \text{ e au}^{-3}$). Electron densities move from the green area to the blue area. Excited states with less than 30000 cm^{-1} and configurations which contribute more than 5% are shown (assignment: H=HOMO; L=LUMO; L+1=LUMO+1; H-1=HOMO-1, etc.).

<p>1</p> <p>403 nm Main Transitions: H-7→L(27%) H-4→L+1(22%) H-6→L+1(7%) H-6→L(7%) H-3→L(7%) H-4→L(5%)</p> <p>$\Phi(^1A \rightarrow ^1A^*) \approx 0.37\Psi_{H-7 \rightarrow L} + 0.32\Psi_{H-4 \rightarrow L+1} - 0.19\Psi_{H-6 \rightarrow L+1} + 0.19\Psi_{H-6 \rightarrow L} - 0.19\Psi_{H-3 \rightarrow L} + 0.16\Psi_{H-4 \rightarrow L}$</p> <p>355 nm Main Transitions: H-7→L(24%) H-4→L+1(17%) H-13→L(11%) H-3→L+4(10%) H-3→L(9%) H-3→L+2(6%)</p> <p>$\Phi(^1A \rightarrow ^1A^*) \approx 0.34\Psi_{H-7 \rightarrow L} - 0.29\Psi_{H-4 \rightarrow L+1} + 0.24\Psi_{H-13 \rightarrow L} - 0.22\Psi_{H-3 \rightarrow L+4} + 0.21\Psi_{H-3 \rightarrow L} - 0.17\Psi_{H-3 \rightarrow L+2}$</p>	<p>394 nm Main Transitions: H-7→L(21%) H-6→L+1(20%) H-7→L+1(18%) H-3→L+2(8%) H-4→L(8%) H-3→L+3(6%)</p> <p>$\Phi(^1A \rightarrow ^1A^*) \approx 0.32\Psi_{H-7 \rightarrow L} + 0.32\Psi_{H-6 \rightarrow L+1} + 0.30\Psi_{H-7 \rightarrow L+1} + 0.20\Psi_{H-3 \rightarrow L+2} - 0.20\Psi_{H-4 \rightarrow L} + 0.17\Psi_{H-3 \rightarrow L+3}$</p> <p>348 nm Main Transitions: H-7→L+1(22%) H-4→L+2(17%) H-4→L(10%) H-3→L+1(7%) H-13→L+1(5%)</p> <p>$\Phi(^1A \rightarrow ^1A^*) \approx 0.33\Psi_{H-7 \rightarrow L+1} - 0.29\Psi_{H-4 \rightarrow L+2} + 0.22\Psi_{H-4 \rightarrow L} + 0.19\Psi_{H-3 \rightarrow L+1} + 0.16\Psi_{H-13 \rightarrow L+1}$</p>
<p>2</p> <p>443 nm Main Transitions: H-7→L(14%) H-4→L+3(12%) H-2→L+3(10%) H-9→L+1(8%) H-1→L+6(7%) H-1→L+4(7%) H-3→L+6(6%)</p> <p>$\Phi(^1A \rightarrow ^1A^*) \approx 0.27\Psi_{H-7 \rightarrow L} - 0.25\Psi_{H-4 \rightarrow L+3} - 0.22\Psi_{H-2 \rightarrow L+3} + 0.20\Psi_{H-9 \rightarrow L+1} + 0.18\Psi_{H-1 \rightarrow L+6} + 0.18\Psi_{H-1 \rightarrow L+4} - 0.17\Psi_{H-3 \rightarrow L+6}$</p>	<p>436 nm Main Transitions: H-2→L+6(22%) H-3→L+5(18%) H-8→L+1(12%) H→L+6(8%) H-5→L+5(7%) H-1→L+3(5%)</p> <p>$\Phi(^1A \rightarrow ^1A^*) \approx 0.33\Psi_{H-2 \rightarrow L+6} - 0.30\Psi_{H-3 \rightarrow L+5} + 0.24\Psi_{H-8 \rightarrow L+1} - 0.19\Psi_{H \rightarrow L+6} + 0.19\Psi_{H-5 \rightarrow L+5} - 0.16\Psi_{H-1 \rightarrow L+3}$</p>

the range of 700–1000 nm (named as region I) originate from the electron transition from the ferrocenyl substituent-centered HOMO(128)/HOMO-1(127)/HOMO-2(126) to the porphyrin core-centered LUMO(129)/LUMO+1(130) for **1**, which is considered as a metal-to-ligand charge transfer (MLCT) transition. The same type of transition in region I also occurs in **2–5**, Fig. 5. The intensity of these MLCT absorptions increases along with increasing the number of ferrocenyl substituents in **1–5**. The porphyrin Q-band absorptions are found in the region of 500–650 nm (named as region II), which originate from the transitions from the highest and second highest occupied porphyrin centered orbitals to LUMO/LUMO+1 orbitals. The Q-band absorptions are found at 585/557 nm for **1**, 601/575 nm for **2** (599/575 nm for **3**), 614/587 nm for **4**, and 631/611 nm for **5**, respectively. The red-shift of the porphyrin Q band along with increasing the number of the *meso*-attached ferrocenyl substituents is in line with the decreasing energy gap between corresponding molecular orbitals as mentioned in Section 3.3.

To clarify the absorptions in the higher energy side of bands of region II (region III), the maps of electron difference between the ground state and excited states for the electron transitions in the region between 300 and 510 nm are shown in Table 3. As long as compound **1** is concerned, all the absorptions in this region are considered as ferrocene → porphyrin electron transitions. Similarly, the absorptions of 443 and 436 nm of **2** also originate from the ferrocene → porphyrin transitions, while the absorptions of 430, 415, and 404 nm originate from the porphyrin → porphyrin transitions. The electron transitions of **3** in this region are considered as ferrocene → ferrocene and porphyrin → porphyrin at

Table 3 (Continued)

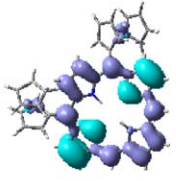
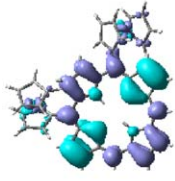
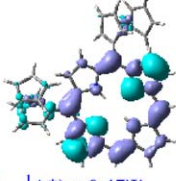
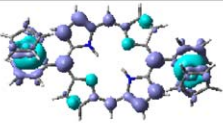
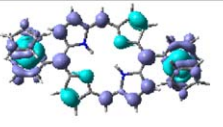
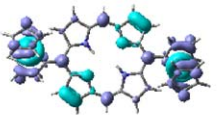
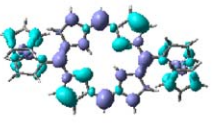
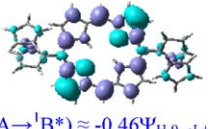
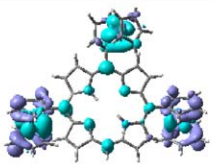
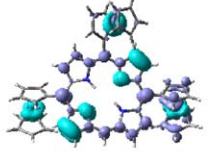
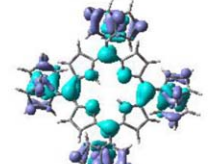
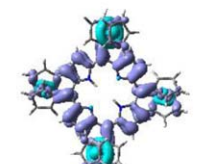
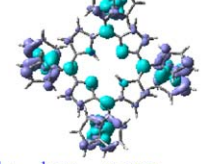
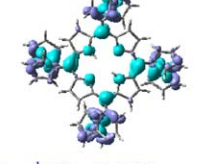
 <p>430 nm Main Transitions: H-8→L(25%) H-9→L(19%) H-6→L+2(7%) H-8→L+1(6%) H-7→L+1(6%) H-9→L+1(6%)</p> $\Phi(^1A \rightarrow ^1A^*) \approx 0.35\Psi_{H-8 \rightarrow L} - 0.31\Psi_{H-9 \rightarrow L} + 0.18\Psi_{H-6 \rightarrow L+2} - 0.18\Psi_{H-8 \rightarrow L+1} + 0.18\Psi_{H-7 \rightarrow L+1} - 0.17\Psi_{H-9 \rightarrow L+1}$	 <p>415 nm Main Transitions: H-9→L(48%) H-6→L+2(18%) H-7→L+1(14%)</p> $\Phi(^1A \rightarrow ^1A^*) \approx 0.49\Psi_{H-9 \rightarrow L} + 0.30\Psi_{H-6 \rightarrow L+2} + 0.26\Psi_{H-7 \rightarrow L+1}$
 <p>404 nm Main Transitions: H-9→L+1(44%) H-7→L(11%) H-11→L(9%) H-6→L+1(6%)</p> $\Phi(^1A \rightarrow ^1A^*) \approx 0.47\Psi_{H-9 \rightarrow L+1} - 0.23\Psi_{H-7 \rightarrow L} - 0.21\Psi_{H-11 \rightarrow L} - 0.17\Psi_{H-6 \rightarrow L+1}$	
<p>3</p>  <p>441 nm Main Transitions: H-1→L+6(17%) H-2→L+3(13%) H-3→L+6(11%) H-4→L+3(11%) H-9→L(10%)</p> $\Phi(^1A \rightarrow ^1A^*) \approx 0.29\Psi_{H-1 \rightarrow L+6} - 0.26\Psi_{H-2 \rightarrow L+3} + 0.24\Psi_{H-3 \rightarrow L+6} + 0.24\Psi_{H-4 \rightarrow L+3} - 0.22\Psi_{H-9 \rightarrow L}$	 <p>428 nm Main Transitions: H-4→L+3(35%) H-1→L+6(23%) H-9→L(8%) H-9→L+1(8%) H-7→L(7%)</p> $\Phi(^1A \rightarrow ^1B^*) \approx 0.42\Psi_{H-4 \rightarrow L+3} - 0.34\Psi_{H-1 \rightarrow L+6} - 0.20\Psi_{H-9 \rightarrow L} + 0.19\Psi_{H-9 \rightarrow L+1} + 0.19\Psi_{H-7 \rightarrow L}$
 <p>425 nm Main Transitions: H-4→L+3(34%) H-9→L+1(12%) H-7→L(11%) H-5→L+4(9%) H-6→L+1(7%)</p> $\Phi(^1A \rightarrow ^1B^*) \approx -0.41\Psi_{H-4 \rightarrow L+3} + 0.25\Psi_{H-9 \rightarrow L+1} + 0.24\Psi_{H-7 \rightarrow L} + 0.21\Psi_{H-5 \rightarrow L+4} + 0.18\Psi_{H-6 \rightarrow L+1}$	 <p>409 nm Main Transitions: H-7→L+1(20%) H-9→L+1(19%) H-15→L(18%) H-6→L+5(5%)</p> $\Phi(^1A \rightarrow ^1B^*) \approx 0.31\Psi_{H-7 \rightarrow L+1} - 0.31\Psi_{H-9 \rightarrow L+1} + 0.30\Psi_{H-15 \rightarrow L} + 0.16\Psi_{H-6 \rightarrow L+5}$
 <p>400 nm Main Transitions: H-9→L+1(43%) H-15→L+1(10%) H-6→L+5(9%)</p> $\Phi(^1A \rightarrow ^1B^*) \approx -0.46\Psi_{H-9 \rightarrow L+1} - 0.23\Psi_{H-15 \rightarrow L+1} - 0.22\Psi_{H-6 \rightarrow L+5}$	

Table 3 (Continued)

<p>4</p>  <p>479 nm Main Transitions: H-0→L+7(58%) H-0→L+6(13%) H-6→L+3(6%)</p> $\Phi(^1A \rightarrow ^1A^*) \approx 0.54\Psi_{H-0 \rightarrow L+7} + 0.25\Psi_{H-0 \rightarrow L+6} + 0.17\Psi_{H-6 \rightarrow L+3}$	<p>451 nm H-10→L(22%) H-12→L(10%) H-10→L+1(9%) H-9→L+1(8%) H-11→L(7%) H-12→L+1(7%)</p> $\Phi(^1A \rightarrow ^1A^*) \approx 0.33\Psi_{H-10 \rightarrow L} - 0.22\Psi_{H-12 \rightarrow L} + 0.21\Psi_{H-10 \rightarrow L+1} + 0.20\Psi_{H-9 \rightarrow L+1} - 0.19\Psi_{H-11 \rightarrow L} + 0.18\Psi_{H-12 \rightarrow L+1}$
 <p>439 nm H-6→L+3(12%) H-12→L(7%) H-5→L+3(7%) H-10→L+1(7%) H-11→L(7%) H-4→L+8(5%) H-6→L+4(5%)</p> $\Phi(^1A \rightarrow ^1A^*) \approx 0.25\Psi_{H-6 \rightarrow L+3} + 0.19\Psi_{H-12 \rightarrow L} - 0.19\Psi_{H-5 \rightarrow L+3} - 0.19\Psi_{H-10 \rightarrow L+1} + 0.19\Psi_{H-11 \rightarrow L} + 0.16\Psi_{H-4 \rightarrow L+8} - 0.16\Psi_{H-6 \rightarrow L+4}$	
<p>5</p>  <p>500 nm Main Transitions: H→L+4(82%) H→L+5(9%)</p> $\Phi(^1A \rightarrow ^1B^*) \approx 0.64\Psi_{H \rightarrow L+4} + 0.22\Psi_{H \rightarrow L+5}$	 <p>490 nm Main Transitions: H-9→L+2(78%) H→L+8(11%)</p> $\Phi(^1A \rightarrow ^1B^*) \approx 0.62\Psi_{H-9 \rightarrow L+2} - 0.24\Psi_{H \rightarrow L+8}$
 <p>487 nm Main Transitions: H→L+8(72%) H-9→L+2(15%)</p> $\Phi(^1A \rightarrow ^1B^*) \approx 0.60\Psi_{H \rightarrow L+8} + 0.28\Psi_{H-9 \rightarrow L+2}$	 <p>482 nm Main Transitions: H→L+9(83%)</p> $\Phi(^1A \rightarrow ^1B^*) \approx 0.64\Psi_{H \rightarrow L+9}$

the same time. The absorption of 479, 451, and 439 nm of **4** originates from the ferrocene → ferrocene, porphyrin → porphyrin, and porphyrin → ferrocene transitions, respectively. In summary, the electron transitions in region III between 300 and 510 nm are complicated. According to the calculation results, this mixed absorption band in this region originates from complicated transitions including the ferrocene → porphyrin, porphyrin → porphyrin, ferrocene → ferrocene, and porphyrin → ferrocene electron transitions.

4. Conclusions

The molecular structures, molecular orbitals, atomic charges, and electronic absorption spectra of a series of *meso*-ferrocenylporphyrins have been comparatively studied by the DFT method. In particular, the orbital coupling has been investigated in detail and the result well explains the long range coupling between ferrocenyl substituents connected via porphyrin core and the systematic change in the electronic absorption spectra of porphyrin compounds due to the coupling of frontier orbitals.

Acknowledgements

Financial support from the Natural Science Foundation of China, Beijing Municipal Commission of Education, and China Post-

doctoral Science Foundation (20090460210 and 201003051) is gratefully acknowledged. We are also grateful to the Shandong Province High Performance Computing Center for a grant of computer time.

Appendix A. Supplementary data

Supplementary data associated with this article can be found, in the online version, at doi:10.1016/j.jmgm.2010.12.006.

References

- [1] M.A. Fox, Fundamentals in the design of molecular electronic devices: long-range charge carrier transport and electronic coupling, *Acc. Chem. Res.* 32 (1999) 201–207.
- [2] C. Joachim, J.K. Gimzewski, A. Aviram, Electronics using hybrid-molecular and mono-molecular devices, *Nature* 408 (2000) 541–548.
- [3] I. Willner, B. Willner, Layered molecular optoelectronic assemblies, *J. Mater. Chem.* 8 (1998) 2543–2556.
- [4] M. Uno, P.H. Dixneuf, Organometallic triskelia: novel tris(vinylideneruthenium(II)), tris(alkynylruthenium(II)), and triruthenium-triferrocenyl complexes, *Angew. Chem., Int. Ed.* 37 (1998) 1714–1717.
- [5] S. Barlow, D. O'Hare, Metal–metal interactions in linked metallocenes, *Chem. Rev.* 97 (1997) 637–670.
- [6] P.D. Beer, P.A. Gale, G.Z. Chen, Mechanisms of electrochemical recognition of cations, anions and neutral guest species by redox-active receptor molecules, *Coord. Chem. Rev.* 185–186 (1999) 3–36.
- [7] A. Ceccon, S. Santi, L. Orian, A. Bisello, Electronic communication in heterobinuclear organometallic complexes through unsaturated hydrocarbon bridges, *Coord. Chem. Rev.* 248 (2004) 683–724.

- [8] E.S. Schmidt, T.S. Calderwood, T.C. Bruice, Synthesis and characterization of a meso-tetrakis(4-ferrocenylphenyl)porphyrin and examination of its ability to undergo intramolecular photocatalyzed electron transfer, *Inorg. Chem.* 25 (1986) 3718–3720.
- [9] K.-W. Poon, W. Liu, P.-K. Chan, Q. Yang, T.-W.D. Chan, T.C.W. Mak, D.K.P. Ng, Tetrapyrrole derivatives substituted with ferrocenylethynyl moieties: synthesis and electrochemical studies, *J. Org. Chem.* 66 (2001) 1553–1559.
- [10] C. Bucher, C.H. Devillers, J.-C. Moutet, G. Royal, E. Saint-Aman, Self-assembly of a ferrocene-substituted porphyrin capable of electrochemically sensing neutral molecules via a “tail on–tail off” process, *Chem. Commun.* (2003) 888–889.
- [11] A. Auger, J.C. Swarts, Synthesis and group electronegativity implications on the electrochemical and spectroscopic properties of diferrocenyl meso-substituted porphyrins, *Organometallics* 26 (2007) 102–109.
- [12] V.N. Nemykin, G.T. Rohde, C.D. Barrett, R.G. Hadt, C. Bizzarri, P. Galloni, B. Floris, I. Nowik, R.H. Herber, A.G. Marrani, R. Zanon, N.M. Loim, Electron-transfer processes in metal-free tetraferrocenylporphyrin: understanding internal interactions to access mixed-valence states potentially useful for quantum cellular automata, *J. Am. Chem. Soc.* 131 (2009) 14969–14978.
- [13] K.-W. Poon, Y. Yan, X.-Y. Li, D.K.P. Ng, Synthesis and electrochemistry of ferrocenylphthalocyanines, *Organometallics* 18 (1999) 3528–3533.
- [14] R.G. Wollmann, D.N. Hendrickson, Synthesis and physical properties of meso-tetraferrocenylporphyrin, the copper complex, and the corresponding mixed-valence coordination products, *Inorg. Chem.* 16 (1977) 3079–3089.
- [15] P.D.W. Boyd, A.K. Burrell, W.M. Campbell, P.A. Cocks, K.C. Gordon, G.B. Jameson, D.L. Officer, Z. Zhao, Bis(ferrocenyl)porphyrins. Compounds with strong long-range metal–metal coupling, *Chem. Commun.* (1999) 637–638.
- [16] A.-C. Ribou, J.-P. Launay, M.L. Sachtleben, H. Li, C.W. Spangler, Intervallence electron transfer in mixed valence diferrocenylpolyenes: decay law of the metal–metal coupling with distance, *Inorg. Chem.* 35 (1996) 3735–3740.
- [17] L. Wan, Y. Zhang, D. Qi, J. Jiang, Structures and properties of 1,8,15,22-tetrasubstituted phthalocyaninato zinc and nickel complexes: substitution and axially coordination effects study based on density functional theory calculations, *J. Mol. Graph. Mod.* 28 (2010) 842–851.
- [18] D. Qi, Y. Zhang, L. Zhang, J. Jiang, Structures and spectroscopic properties of fluoroboron-substituted porphyrin derivatives: density functional theory approach on the benzo-fusing effect, *J. Phys. Chem. A* 114 (2010) 1931–1938.
- [19] D. Qi, Y. Zhang, X. Cai, J. Jiang, M. Bai, Inner hydrogen atom transfer in benzo-fused low symmetrical metal-free tetraazaporphyrin and phthalocyanine analogues: density functional theory studies, *J. Mol. Graph. Mod.* 27 (2009) 693–700.
- [20] Y. Zhang, X. Cai, P. Yao, H. Xu, Y. Bian, J. Jiang, Location of the hole and acid proton in neutral nonprotonated and protonated mixed (phthalocyaninato)(porphyrinato) yttrium double-decker complexes: density functional theory calculations, *Chem. Eur. J.* 13 (2007) 9503–9514.
- [21] G.D. Luca, A. Romeo, L.M. Scolaro, G. Ricciardi, A. Rosa, A. Rosa, Sitting-atop metallo-porphyrin complexes: experimental and theoretical investigations on such elusive species, *Inorg. Chem.* 48 (2009) 8493–8507.
- [22] G.A. Peralta, M. Seth, T. Ziegler, Magnetic circular dichroism of porphyrins containing M = Ca, Ni, and Zn. A computational study based on time-dependent density functional theory, *Inorg. Chem.* 46 (2007) 9111–9125.
- [23] V.N. Nemykin, R.G. Hadt, R.V. Belosludov, H. Mizuseki, Y. Kawazoe, Influence of molecular geometry, exchange-correlation functional, and solvent effects in the modeling of vertical excitation energies in phthalocyanines using time-dependent density functional theory (TDDFT) and polarized continuum model TDDFT methods: can modern computational chemistry methods explain experimental controversies? *J. Phys. Chem. A* 111 (2007) 12901–12913.
- [24] V.N. Nemykin, A.Y. Maximov, A.Y. Kopysov, Mercury-free preparation, characterization, and molecular structure of tricyanovinylferrocene using an unusual reaction between ferrocene and tetracyanoethylene, *Organometallics* 26 (2007) 3138–3148.
- [25] V.N. Nemykin, R.G. Hadt, Influence of Hartree–Fock exchange on the calculated Mössbauer isomer shifts and quadrupole splittings in ferrocene derivatives using density functional theory, *Inorg. Chem.* 45 (2006) 8297–8307.
- [26] V.N. Nemykin, E.A. Makarova, J.O. Grosland, R.G. Hadt, A.Y. Kopysov, Preparation, characterization, molecular and electronic structures, TDDFT, and TDDFT/PCM study of the solvatochromism in cyanovinylferrocenes, *Inorg. Chem.* 46 (2007) 9591–9601.
- [27] R.H. Herber, I. Nowik, J.O. Grosland, R.G. Hadt, V.N. Nemykin, *J. Organomet. Chem.* 693 (2008) 1850–1856.
- [28] S. Santi, L. Orian, A. Donoli, A. Bisello, M. Scapinello, F. Benetollo, P. Ganis, A. Ceccon, Synthesis of the prototypical cyclic metallocene triad: mixed-valence properties of [(FeCp)₃(trindenyl)] isomers, *Angew. Chem., Int. Ed.* 47 (2008) 5331–5334.
- [29] S. Santi, L. Orian, C. Durante, E.Z. Bencze, A. Bisello, A. Donoli, A. Ceccon, F. Benetollo, L. Crociani, Metal–metal electronic coupling in syn- and anti-stereoisomers of mixed-valent (FeCp)²⁺, (RhL₂)²⁺, and (FeCp)(RhL₂)-as-indacenediide ions, *Chem. Eur. J.* 13 (2007) 7933–7947.
- [30] V.N. Nemykin, G.T. Rohde, C.D. Barrett, R.G. Hadt, J.R. Sabin, G. Reina, P. Galloni, B. Floris, Long-range electronic communication in free-base meso-poly(ferrocenyl)-containing porphyrins, *Inorg. Chem.* 49 (2010) 7497–7509.
- [31] V.N. Nemykin, R.G. Hadt, Interpretation of the UV–vis spectra of the meso(ferrocenyl)-containing porphyrins using a TDDFT approach: is Gouterman’s classic four-orbital model still in play? *J. Phys. Chem. A* 114 (2010) 12062–12066.
- [32] A.D. Becke, Density-functional thermochemistry. III. The role of exact exchange, *J. Chem. Phys.* 98 (1993) 5648–5652.
- [33] C. Lee, W. Yang, R.G. Parr, Development of the Colle–Salvetti correlation-energy formula into a functional of the electron density, *Phys. Rev. B* 37 (1988) 785–789.
- [34] S. Shaik, D. Kumar, S.P. de Visser, A. Altun, W. Thiel, Theoretical perspective on the structure and mechanism of cytochrome P450 enzymes, *Chem. Rev.* 105 (2005) 2279–2328.
- [35] P.J. Hay, W.R. Wadt, Ab initio effective core potentials for molecular calculations. Potentials for the transition metal atoms Sc to Hg, *J. Chem. Phys.* 82 (1985) 270–283.
- [36] C. Peng, P.Y. Ayala, H.B. Schlegel, M.J. Frisch, Using redundant internal coordinates to optimize equilibrium geometries and transition states, *J. Comput. Chem.* 17 (1996) 49–56.
- [37] A.E. Reed, L.A. Curtiss, F. Weinhold, Intermolecular interactions from a natural bond orbital, donor–acceptor viewpoint, *Chem. Rev.* 88 (1988) 899–926.
- [38] J.E. Carpenter, F. Weinhold, Analysis of the geometry of the hydroxymethyl radical by the “different hybrids for different spins” natural bond orbital procedure, *J. Mol. Struct. (THEOCHEM)* 169 (1988) 41–62.
- [39] M.J. Frisch, G.W. Trucks, H.B. Schlegel, G.E. Scuseria, M.A. Robb, J.R. Cheeseman, J.A. Montgomery Jr., T. Vreven, K.N. Kudin, J.C. Burant, J.M. Millam, S.S. Iyengar, J. Tomasi, V. Barone, B. Mennucci, M. Cossi, G. Scalmani, N. Rega, G.A. Petersson, H. Nakatsuji, M. Hada, M. Ehara, K. Toyota, R. Fukuda, J. Hasegawa, M. Ishida, T. Nakajima, Y. Honda, O. Kitao, H. Nakai, M. Klene, X. Li, J.E. Knox, H.P. Hratchian, J.B. Cross, V. Bakken, C. Adamo, J. Jaramillo, R. Gomperts, R.E. Stratmann, O. Yazyev, A.J. Austin, R. Cammi, C. Pomelli, J.W. Ochterski, P.Y. Ayala, K. Morokuma, G.A. Voth, P. Salvador, J.J. Dannenberg, V.G. Zakrzewski, S. Dapprich, A.D. Daniels, M.C. Strain, O. Farkas, D.K. Malick, A.D. Rabuck, K. Raghavachari, J.B. Foresman, J.V. Ortiz, Q. Cui, A.G. Baboul, S. Clifford, J. Cioslowski, B.B. Stefanov, G. Liu, A. Liashenko, P. Piskorz, I. Komaromi, R.L. Martin, D.J. Fox, T. Keith, M.A. Al-Laham, C.Y. Peng, A. Nanayakkara, M. Challacombe, P.M.W. Gill, B. Johnson, W. Chen, M.W. Wong, C. Gonzalez, J.A. Pople, Gaussian03, Revision B.05, Gaussian, Inc., Pittsburgh, PA, 2003.
- [40] J.P. Perdew, Y. Wang, Accurate and simple analytic representation of the electron–gas correlation energy, *Phys. Rev. B* 45 (1992) 13244–13249.
- [41] K.S. Suslick, C. Chen, G.R. Meredith, L. Cheng, Push–pull porphyrin as nonlinear optical materials, *J. Am. Chem. Soc.* 114 (1992) 6928–6930.
- [42] R. Koerner, J.L. Wright, X.D. Ding, M.J.M. Neset, K. Aubrecht, R.A. Watson, R.A. Barber, L.M. Mink, A.R. Tipton, C.J. Norvell, K. Skidmore, U. Simonis, F.A. Walker, Electronic effects in transition metal porphyrins. 9. Effect of phenyl ortho substituents on the spectroscopic and redox properties and axial ligand binding constants of iron(III) tetraphenylporphyrins, *Inorg. Chem.* 37 (1998) 733–745.
- [43] V.N. Nemykin, P. Galloni, B. Floris, C.D. Barrett, R.G. Hadt, R.I. Subbotin, A.G. Marrani, R. Zanon, N.M. Loim, Metal-free and transition-metal tetraferrocenylporphyrins part 1: synthesis, characterization, electronic structure, and conformational flexibility of neutral compounds, *Dalton Trans.* (2008) 4233–4246.
- [44] J. Vura-Weis, M.A. Ratner, M.R. Wasielewski, Geometry and electronic coupling in peryleneimide stacks: mapping structure–charge transport relationships, *J. Am. Chem. Soc.* 132 (2010) 1738–1739.